Nonlinear Dynamics of Microwave Synthesizers—Stability and Noise

Sergio Sancho, Almudena Suárez, *Member, IEEE*, and Tomás Fernández

***Abstract*—The nonlinear dynamics of microwave synthesizers based on type-II third-order loops is analyzed in this paper. Instead of using standard simplified models, realistic models are considered for the loop filter, phase detector (PD), and voltage-controlled oscillator based on experimental characterization. The new models enable the simulation of incidental frequency modulation and the accurate prediction of the synthesizer operation ranges, including possible hysteresis phenomena. The stability of phase-locked solutions is analyzed, enabling the prediction of possible chaotic behavior. For an accurate determination of the output spectrum, a phase-noise simulation is also carried out, considering the noise contributions from the loop elements. The sidebands inherent to the synthesizer solution are taken into account for this analysis. All the above analysis strategy has been applied to a microwave synthesizer, operating in the 2–3-GHz band, with very good results. Two types of PDs are considered: the JK flip-flop PD and frequency mixer, comparing the resulting loop performance in terms of stability and phase noise.**

***Index Terms*—Chaos, hysteresis, incidental FM, microwave synthesizers, phase noise, stochastic resonance.**

I. Introduction

THE strict phase-noise specifications of current communication systems usually make necessary the synthesis of microwave oscillators before their integration in a particular system. This frequency synthesis is carried out through a phase-locked loop (PLL). The main elements of this loop, aside from the voltage-controlled oscillator (VCO), are the phase detector (PD) (which may be analog or digital), loop filter, and frequency divider (Fig. 1). For phase-noise reduction, the convenience of using a type-II (or higher) PLL has been shown [1]. Actually, the type-II third-order PLL, with an integrator in the filter loop (the other is provided by the VCO transfer function) is the most common type of synthesizer at microwave frequencies. Although more poles may be added to the loop filter for reference suppression, the type-II third-order PLL provides a good insight into the system nonlinear dynamics [1].

In the linear analysis of the synthesizer, the PD is modeled with a linear function. However, this simplification is only valid for small phase error between the two input signals. The actual nonlinear nature of this and other elements, together with the system feedback, often give rise to very complex nonlinear behavior. Actually, some works [2], [3] relate the type-I PLL equations to those describing the Josephson-junction superconductor [4], for which the existence of chaotic attractors has been analytically demonstrated.

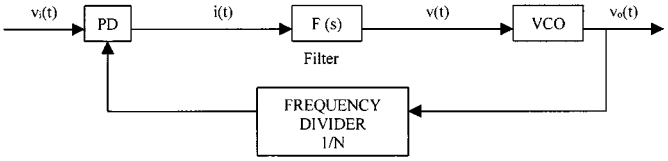

Fig. 1. Schematic of the frequency synthesizer.

Most of the studies on PLL nonlinear dynamics are devoted to type-I PLLs [2], [3]. In the case of type-II PLLs, infinitum hold-in ranges are theoretically obtained [1], [5], [6] due to the presence of a second integrator in the loop. The fact that the synthesizer is always in locked condition should also prevent any hysteresis or instability phenomenon. However, this contradicts the everyday observations of microwave-oscillator designers.

The nonlinear analysis is the first step for a realistic prediction of the behavior of the microwave synthesizer. This nonlinear analysis, introduced, among others, by Viterbi [7] and Sanneman *et al.* [8] provided invaluable information about the basic operation of second- and third-order loops. However, even in a nonlinear analysis, the results may qualitatively differ from the experimental ones if oversimplified descriptions are taken for the loop elements. Actually, when using simplified models for the response of the PD (as a function of the phase difference between its two input signals), the prediction, for instance, of the incidental frequency modulation (FM) [1] is impossible. In locked condition, these models provide a constant frequency and a constant phase shift in the VCO output when experimental observations show a frequency modulation of this signal. In the spectrum, this gives rise to sidebands, which are inherent to the synthesizer solution. The variation in the actual nature of the steady-state solution may invalidate the stability predictions of the standard linearization around a constant-phase solution. In fact, instabilities of the frequency-modulated solution may lead to chaotic behavior [9]. On the other hand, the FM sidebands influence the overall phase-noise behavior of the synthesizer and should be taken into account when designing under strict phase-noise specifications.

The aim of the analysis presented in this paper has been to gain some insight into the nonlinear dynamics of microwave synthesizers based on type-II loops. The analysis is based on realistic descriptions of the synthesizer elements. The capability to determine and detect the instability phenomena that lead the

Manuscript received August 2, 2000. The work of S. Sancho was supported by the Basque Government. The work of A. Suárez was supported by the Fondos Europeos para el Desarrollo Regional under Project IFD97-0455-C02-01.

S. Sancho is with the Electronic Engineering Department, University of Santander, 39005 Santander, Spain.

A. Suárez and T. Fernández are with the Communications Engineering Department, Escuela Técnica Superior de Ingenieros Industriales y de Telecomunicación, University of Cantabria, 39005 Santander, Spain.

Publisher Item Identifier S 0018-9480(01)08686-0.

system out of lock should enable an accurate prediction of its operation ranges. In order to evaluate the influence of noise perturbations on the actual system solution, the phase-noise contributions of the loop elements, obtained from experimental characterization, have also been considered. The synthesizer phase-noise analysis is carried out taking into account the actual oscillating nature of the solution. This accurate prediction of the phase-noise spectrum should also avoid the usual laboratory trial-and-error work before obtaining satisfactory result. For the sake of generality, two different types of PD have been considered: an analog mixer and a JK flip-flop PD.

The paper is organized as follows. Section II presents the synthesizer equations and the element models that have been used here, comparing the simulation results with those obtained through traditional modeling. Section III shows a parametric analysis of the synthesizer, with emphasis on the determination of its operating limits. Section IV analyzes the synthesizer stability and the presence of chaotic solutions. Section V is devoted to the analysis of the synthesizer phase-noise. The analysis is particularized to a 2–3-GHz microwave synthesizer and, in each section, simulation results are compared with measurements.

II. Nonlinear Modeling of the Microwave Synthesizer

A. Synthesizer General Equations

As shown in Fig. 1, the synthesizer is made up of a nonlinear PD, a loop filter, a VCO, and a frequency divider. The input-signal $\mathrm{v_i}(\mathrm{t})$ is considered to be a sinusoidal waveform, given by

$$\mathrm{v_i}(\mathrm{t}) = \cos[\theta_{\mathrm{i}}(\mathrm{t})], \qquad \text{with } \theta_{\mathrm{i}}(\mathrm{t}) \in \mathbf{S}^1 \text{ and } \frac{\mathrm{d}\theta_{\mathrm{i}}}{\mathrm{dt}} = \omega_i \tag{1}$$

while the VCO output has the form

$$\mathrm{v_o}(\mathrm{t}) = \cos[\theta_{\mathrm{o}}(\mathrm{t})], \qquad \theta_{\mathrm{o}}(\mathrm{t}) \in \mathbf{S}^1. \tag{2}$$

The output current of the PD is a nonlinear function of both the input phase θ_{i} and the output phase θ_{o} (divided by N)

$$\mathrm{i}(\mathrm{t}) = \mathrm{h}\left[\theta_{\mathrm{i}}(\mathrm{t}),\ \frac{\theta_{\mathrm{o}}(t)}{\mathrm{N}}\right]. \tag{3}$$

In the particular case of a type-II third-order loop, the filter transfer function is given by

$$\mathrm{F(s)} = \frac{\tau_1 \mathrm{s} + 1}{\tau_2 \mathrm{s}(\tau_3 \mathrm{s} + 1)}. \tag{4}$$

The pole ideally located at the origin provides high dc gain and improves the phase-noise characteristic. The VCO oscillates at a frequency depending on the control voltage $\mathrm{v}(\mathrm{t})$

$$\dot{\theta}_o(t) = \mathrm{f_{VCO}}[\mathrm{v}(\mathrm{t})]. \tag{5}$$

The phase-detector output current $\mathrm{i}(\mathrm{t})$ and the control voltage $\mathrm{v}(\mathrm{t})$ are related by the filter transfer function

$$\mathrm{V(s)} = \mathrm{F(s)I(s)}. \tag{6}$$

The combination of equations from (3)–(6) provides the Laplace form of the general equation governing the synthesizer dynamics

$$s\theta_o = \mathrm{f_{VCO}}\left[\mathrm{F(s)I}\left(\theta_i,\ \frac{\theta_o}{\mathrm{N}}\right)\right]. \tag{7}$$

Since $\theta_{\mathrm{i}}(\mathrm{t})$ only depends on time, the synthesizer can be modeled as a time varying (time dependent) third-order system whose state variables are the VCO output phase and its first- and second-order time derivatives $(\theta_{\mathrm{o}}, \dot{\theta}_{\mathrm{o}}, \ddot{\theta}_{\mathrm{o}})$. This is the most general description of the synthesizer. Now the general functions from (3)–(5) are going to be replaced with realistic models.

B. Description of the Filter

In (4), the filter response is modeled with an ideal transfer function, having a pole located exactly at the origin. However, this location is not possible in practice, due to dc gain finiteness and parasitics in the active filter. Actually, for this situation, the system becomes a stability *center* for the unlocked rotation solutions, as in a linear oscillator. In a more realistic description of the filter, the pole will be slightly displaced from the origin, according to the actual element values. The ratio between the two pole displacements remains, however, very small. The new transfer function is given by

$$\mathrm{F(s)} = \frac{\tau_1 \mathrm{s} + 1}{\tau_2 \tau_3 (\mathrm{s}^2 + \mathrm{Bs} + \mathrm{C})} \tag{8}$$

where B and C are constant coefficients, calculated so that the zero (at $1/\tau_1$) and pole (at $1/\tau_3$) remain at the same positions of (4). The second pole (very close to the origin) is estimated from the actual filter response. This pole is located at $\varepsilon(\mathrm{B}, \mathrm{C})$. As will be shown, the value ε has a great influence on the system dynamics.

C. Description of the VCO Response

For an accurate simulation of the synthesizer behavior, a realistic model of the VCO response versus the control voltage must be considered. This model must include all the saturation and nonlinear effects observed in this circuit. The linear approximation often considered in PLL analysis is valid for small variations of the control voltage $\mathrm{v}(\mathrm{t})$, but in the general case, is inaccurate. As an example, the VCO employed here has been experimentally characterized, obtaining the frequency response of Fig. 2. A curve of this type can be modeled with the following equation:

$$\dot{\theta}_{\mathrm{o}}(t) = \omega_o + k_1 \mathrm{tgh}[k_v\, v(t)] \tag{9}$$

where $\mathrm{k_1}$ and $\mathrm{k_v}$ are fitting parameters and ω_{o} is the free-running angular frequency of the VCO. The modeled characteristic has been superimposed over the experimental one (see Fig. 2).

D. Description of the PD

Two different kinds of PD (i.e., analog and digital, respectively) have been considered here: a frequency mixer and a JK flip-flop, as an example of digital PD. The objective has been the analysis and comparison of the overall system dynamics, when

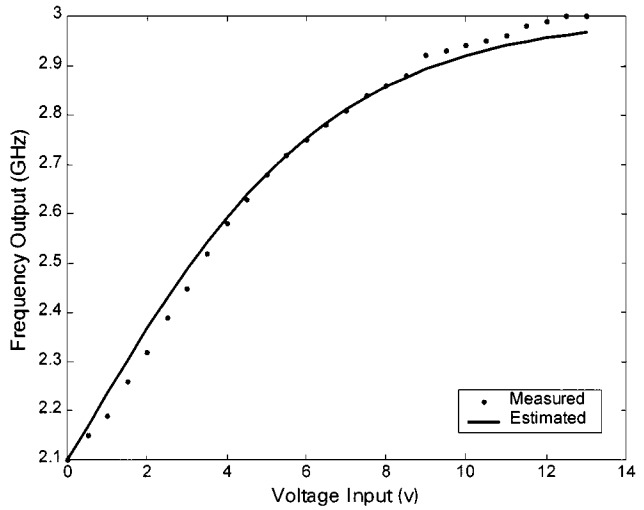

Fig. 2. Frequency response of the VCO versus the control voltage. The parameters of (9) are $k_1 = 5.7\ 10^9$ rad/s, $k_v = 0.15\ v^{-1}$, $\omega_0 = 2.1 \cdot 2\pi\ 10^9$ rad/s.

using two different types of PDs, and the JK has been chosen for modeling simplicity. The tristate comparator is also widely used and will be the object of a future work.

1) Frequency Mixer: The frequency mixer is a nonlinear element, giving rise to intermodulation products of the two input frequencies. The products with highest amplitude correspond to the lowest intermodulation orders. For the sake of simplicity, in classic PLL analysis (even in nonlinear analysis), the response of the frequency mixer is generally limited to the phase-difference term. In this approximation, it is assumed that the phase-sum term is completely attenuated by the low-pass filter. Under this assumption, the equation for the PD output current (3) is reduced to

$$\begin{aligned} i(t) &= h\left[\theta_i(t) - \frac{\theta_o(t)}{N}\right] \\ &= k_d \cos\left[\theta_i(t) - \frac{\theta_o(t)}{N}\right] \\ &= k_d \cos[\phi(t)] \end{aligned} \tag{10}$$

where k_d is the phase-detector output current and $\phi(t)$ is the so-called *phase error*.

In order to get some insight into the influence of the intermodulation products, the term corresponding to phase addition has been included in the PD model

$$i(t) = k_d\left[\cos\left(\theta_i - \frac{\theta_o}{N}\right) + \cos\left(\theta_i + \frac{\theta_o}{N}\right)\right]. \tag{11}$$

2) JK-Based PD: A JK flip-flop has been chosen as an example of digital PD, due to its accurate detection of both phase and frequency variations [1]. In this kind of detector, there are two output levels. The output current is positive in two cases: when the reference frequency is bigger than the output frequency divided by N and, if the two frequencies have the same value, when the reference signal leads the frequency-divided output signal in phase. In the opposite cases, the output current is negative. The filter capacitor is charged for the positive level and discharged for the negative one. The filter integrator averages the PD output pulses. Taking into account this averaging of the current pulses, the JK PD has usually been modeled with the *sawtooth* equation

$$i(t) = k_d\phi(t), \qquad \text{with } \phi(t) \in \mathbf{S}^1. \tag{12}$$

In this study, the sequential character of the output current has been taken into account to enable a more accurate modeling. The *table of truth* of the JK flip-flop provides the following piecewise-linear function:

$$\begin{aligned} i_n &= h\left(\theta_{i_n}, \frac{\theta_{o_n}}{N}, \theta_{i_{n-1}}, \frac{\theta_{o_{n-1}}}{N}\right) \\ i_n &= +K_d, \qquad \text{for } \theta_{i_{n-1}} \in (0, \pi) \text{ and } \theta_{i_n} \in (\pi, 2\pi) \\ i_n &= -K_d, \qquad \text{for } \frac{\theta_{o_{n-1}}}{N} \in (0, \pi) \text{ and } \frac{\theta_{o_n}}{N} \in (\pi, 2\pi) \\ i_n &= i_{n-1}, \qquad \text{for any other case.} \end{aligned} \tag{13}$$

It is a discontinuous function with a memory. Note that the output current depends on both the divider output phase θ_o/N and the reference phase θ_i. Its highly nonlinear dynamics gives rise to many spurious terms, resulting from intermodulation. These spurious terms have a crucial influence on the synthesizer dynamics, as will be shown.

III. Global Analysis of the Synthesizer Nonlinear Dynamics

In this section, the general equation (7) governing the synthesizer dynamics is particularized to the case of using a frequency mixer or a JK PD.

A. Synthesizer With an Analog PD—Frequency Mixer

In order to show the relevance of the phase-detector model in the system dynamics, both the simplified description of the frequency mixer given by (10) and the more accurate one given by (11) will be considered.

1) Time-Invariant Case: When using the simplified description (10), the synthesizer equations can be globally expressed in terms of the phase error

$$\begin{aligned} \ddot{v} + B\dot{v} + Cv &= \frac{\tau_1}{\tau_2\tau_3}\frac{di}{dt} + \frac{1}{\tau_2\tau_3} i \\ &= -\frac{\tau_1 k_d}{\tau_2\tau_3}\dot{\phi}\sin(\phi) + \frac{k_d}{\tau_2\tau_3}\cos(\phi) \\ \dot{\phi}(t) &= \frac{\Delta\omega}{N} - \frac{k_1}{N}\,\mathrm{tgh}[k_v v(t)] \end{aligned} \tag{14}$$

where $\Delta\omega = N\omega_i - \omega_o$. The cases $\Delta\omega \geq 0$ and $\Delta\omega \leq 0$ are symmetric, thus, only N values making $\Delta\omega \geq 0$ will be considered.

The system (14) is time invariant since its equations do not depend explicitly on time. The state variables are given by $(\phi, \dot{\phi}, \ddot{\phi})$. Since the system is periodic in ϕ, every system state is an element of $(S^1 \times R \times R)$.

When solving (14), the main interest is in finding the phase-locked solutions and the parameter ranges for which these solutions exist. When writing the synthesizer equation in terms of the phase error [as has been done in (14)], these phase-locked

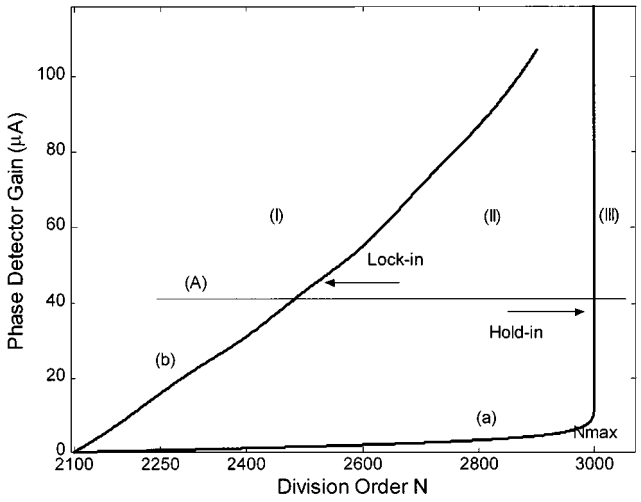

Fig. 3. Bifurcation diagram of the synthesizer when a frequency mixer is used as a PD.

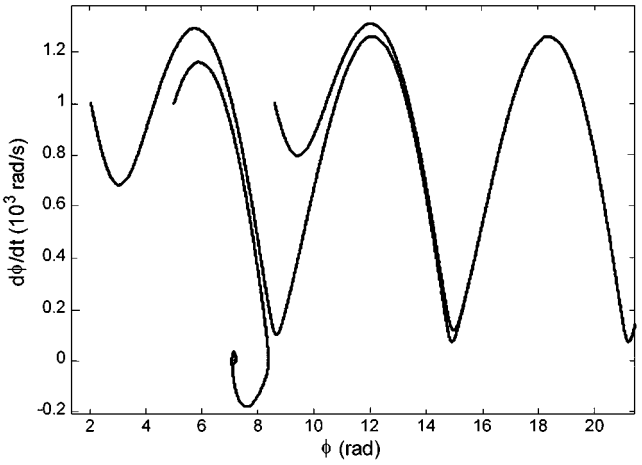

Fig. 4. Synthesizer based on a frequency mixer. Autonomous system. Coexistence, for the same parameter values, of a stable phase-locked solution (EP) and a stable rotation solution.

solutions are given by a constant phase-error value $\phi = \phi_o$. Thus, they correspond to the equilibrium points (EPs) of the time-invariant system (14), which are calculated by equating $(\dot{\phi}, \ddot{\phi}) = (0, 0)$. This provides

$$\sin(\phi) = \frac{\tau_2 \tau_3 C}{2k_d} \ln \frac{k_1 + \Delta\omega}{k_1 - \Delta\omega}. \tag{15}$$

The existence of EPs is determined by the condition $|\sin\phi| \leq 1$. Thus, the EPs or the phase-locked solutions do not exist for all the parameter values. The parameters that will be considered here are the PD current $\mathrm{k_d}$ and the division order N, both included in (15). When the condition $|\sin\phi| \leq 1$ is fulfilled, two different solutions are obtained, i.e., (ϕ_{on}, ϕ_{os}). These solutions correspond to locked states of the system since the frequency error $\dot{\phi}$ is zero. The relation between both solutions is $\phi_{\mathrm{on}} = \pi - \phi_{\mathrm{os}}$. It can be shown that one of the solutions, i.e., ϕ_{on}, is a stable focus of node type and ϕ_{os} is an unstable solution of saddle type. Since one of the filter poles is very close to the origin, ϕ_{n} will have a value close to zero for most of the parameter-variation range. Its value will vary fast for parameter values near the limit condition $|\sin(\phi)| = 1$.

In the plane defined by $\mathrm{k_d}$ and N, the curve delimiting the existence of phase-locked solutions is obtained from the condition $|\sin(\phi)| = 1$

$$k_d = \frac{\tau_2 \tau_3 C}{2} \ln \frac{k_1 + \Delta\omega}{k_1 - \Delta\omega}. \tag{16}$$

Note that since $\Delta\omega \leq \mathrm{k_1}$ [due to (9)], the quantity inside the logarithm is always positive. The curve given by (16) has been represented in Fig. 3 [curve (a)]. Phase-locked solutions only exist on the left-hand side of curve (a), this curve providing the synthesizer *hold-in* range. Along curve (a), a collision between the stable and unstable EPs $(\phi_{\mathrm{on}}, \phi_{\mathrm{os}})$ takes place. This collision gives rise to the extinction or creation (according to the sense of variation of the parameter) of the two EPs in a *saddle-node* bifurcation [10]. Note that for $\Delta\omega \to \mathrm{k_1}$, the current $\mathrm{k_d}$ tends to infinitum, which means that beyond this limit, locking is not possible. This is due to the VCO saturation. The parameter N can never increase beyond a maximum value $N_{\max}$ corresponding to the maximum frequency at which the VCO can oscillate before saturation. Here, the maximum VCO output frequency is $\omega_{\mathrm{o}} + \mathrm{k_1}$ [from (9)], thus, the maximum integer product of the input frequency that can be followed by the VCO is $N_{\max}\omega_i = \omega_o + k_1$. Therefore, $\mathrm{N_{max}}$ limits the bifurcation diagram.

Up to now, (14) has only been solved for its EPs. However, for some parameter ranges, a time periodic solution may also be found. This is a stable periodic orbit $\phi_{\mathrm{r}}(\mathrm{t})$ of rotation type [2]–[4] that has the property

$$\dot{\phi}_r(t) > 0 \qquad \forall t. \tag{17}$$

This solution has been represented in Fig. 4 for parameter values $(\mathrm{N}, \mathrm{k_d})$ for which it coexists with the EP. Note that great time variations of the frequency error are obtained for this solution. Since the frequency error is always positive, the VCO output frequency never locks to $\mathrm{N}\omega_{\mathrm{i}}$. Thus, the rotation solution will correspond to an unlocked state of the system. The rotation solution typically originates at the saddle EP, through the nontransversal intersection of its stable and unstable manifolds [10]. This phenomenon occurs for $(\mathrm{k_d}, \mathrm{N})$ values, forming a curve in the parameter plane that cannot be analytically obtained for the complex system (14). Along this curve (curve (b) of Fig. 3), the periodic solution $\phi_{\mathrm{r}}(\mathrm{t})$ collides with the unstable EP. The phenomenon is called *saddle connection* [2]–[4]. This provides the *lock-in* border in the synthesizer operation. The two curves respectively given by the *saddle-node* bifurcation [curve (a)] and the *saddle connection* [curve (b)] define three different regions in the parameter plane. In region I, there are two EPs. In region II, EPs and rotation solutions coexist and, according to the system initial values, convergence to an EP or a rotation solution may be obtained, as shown in Fig. 4. In region III, there are rotation solutions.

As has been pointed out, the distance to the origin of the second filter pole is a very sensitive parameter in the system dynamics. Actually, the position of the stability borders greatly depends on this parameter. For $\varepsilon = 0$, the *saddle-node*-bifurcation curve lies on the horizontal axis and the *hold-in* range becomes infinite, in agreement with analytical predictions from

simplified models [5], [6]. The *saddle-connection* border also approaches the horizontal N axis when the distance ε is decreased.

The sequence of bifurcations obtained when increasing N for constant $\mathrm{k_d}$ (following the horizontal line (A) of the bifurcation diagram of Fig. 3) is described below. Initially, the system operates in region I and the solution trajectory evolves to the stable node. At this point, the PLL is locked. If N is now increased, the system enters region II and the rotation solution appears and coexists with the EPs. However, since the system is moving from region I, its initial conditions are close to the stable EP and the system remains locked. Continuing to increase N, as curve (a) is approached, the stable and unstable EPs approach each other fast and eventually collide. In region III, the EPs have disappeared and the system trajectory is attracted by the stable rotation solution, the synthesizer becoming unlocked. Now, if line A is followed in the inverse sense (from region III to region I), a hysteresis phenomenon is observed. Actually, when reducing the N value, curve (a) is traversed, the two EPs reappear, but the initial conditions, very close to the rotation solution, make the system trajectory converge to solutions of rotation type. Thus, the system remains unlocked in a parameter region for which locked solutions had previously been obtained. However, as N continues to be reduced, the amplitude of the rotation increases and a collision with the unstable EP takes place at the *saddle-connection* curve [curve (b)]. After this collision, the rotation is destroyed. The system enters region I and the solution trajectory is attracted by the stable node (the only stable solution). When this happens, the system gets locked.

2) Time Varying Case: When the phase sum term, neglected in (10), is taken into account for the synthesizer analysis, important qualitative variations are obtained in its dynamics. When considering this term, the synthesizer equation becomes

$$\begin{aligned}\ddot{v}+B\dot{v}+Cv &= \frac{\tau_1}{\tau_2\tau_3}\frac{di}{dt}+\frac{1}{\tau_2\tau_3}\,i \\ &= -\frac{\tau_1 k_d}{\tau_2\tau_3}\left[\dot{\phi}\sin\phi+\left(2\omega_i-\dot{\phi}\right)\sin\left(2\omega_i t-\phi\right)\right] \\ &\quad +\frac{k_d}{\tau_2\tau_3}\left[\cos\phi+\cos\left(2\omega_i t-\phi\right)\right] \\ \dot{\phi}(t) &= \frac{\Delta\omega}{N}-\frac{k_1}{N}\,\mathrm{tgh}\left[k_v v(t)\right]. \end{aligned} \tag{18}$$

This is a time-varying (time-dependent) system of the form

$$\dot{\overline{x}}(t)=\mathbf{F}\left[\overline{x}(\mathrm{t}),\,\mathrm{t}\right] \tag{19}$$

where $\overline{\mathrm{X}}$ is the vector of state variables and F is the vector of nonlinear functions.

Equation (18) is T-periodic in the variable t with $T=\pi/\omega_i$, being half the period of the external forcing. This is due to the model of the PD, which now includes the phase addition term. By averaging (18) in the variable t over one period T, a system identical to (14) is obtained. Actually, the system (14) agrees with the *time-invariant averaged system* associated to (18) [10] since it has been obtained by averaging (18). It can be shown [10] that, for small values of the ratio $\mathrm{k_d/N}$, the EPs of the averaged system become limit cycles of period T, with the same stability properties as the EPs of system (14) [10]. In practice, this assumption is valid for the whole range of $(\mathrm{k_d},\,\mathrm{N})$ values that are usually covered in the performance of the synthesizer based on the frequency mixer. Thus, the bifurcation diagram for the system (18) has the same regions as the one shown before (Fig. 3). It must also be noted that the rotation-type periodic solutions of the averaged system (14) become quasi-periodic solutions of (18), with fundamental frequencies given by the self-oscillation frequency [observed in the rotations of the system (14)] and the frequency $2\omega_\mathrm{i}$. The two types of more realistic solutions (limit cycle and quasi-periodic rotation) are shown in Fig. 5. Note that now the locked states are not EPs in the space $(\mathrm{S}^1\times\mathrm{R}\times\mathrm{R})$, but limit cycles surrounding the EPs of (14). Thus, the output $\mathrm{v_o(t)}$ of the VCO in the locked state is frequency modulated at $2\omega_\mathrm{i}$. This will originate spurious frequency components on each side of the carrier, with an amplitude proportional to the amplitude of the stable limit cycle. This amplitude grows with the phase-detector current $\mathrm{k_d}$ and decreases with the parameter N.

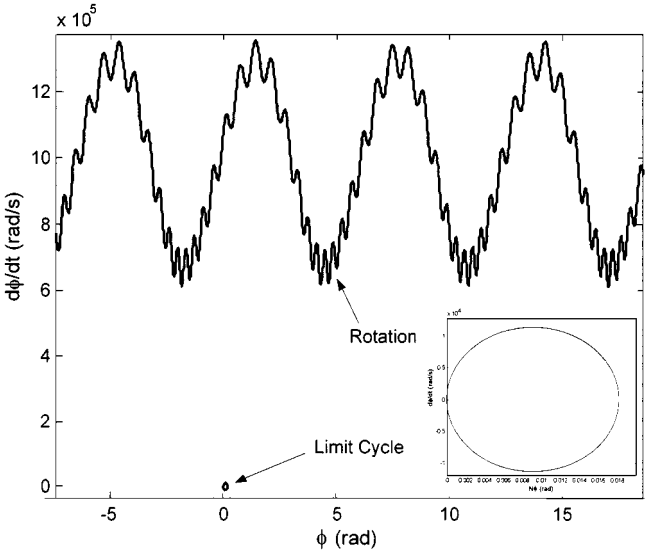

Fig. 5. Synthesizer based on a frequency mixer. Time-varying system. Coexistence, for the same parameter values, of a stable phase-locked solution (limit cycle) and a stable rotation solution (quasi-periodic). Inset: expanded view of the limit cycle.

Note that the inclusion of further intermodulation terms in the phase-detector response would give rise to more complex dynamics. This is shown in the second type of PD that has been considered here: i.e., the JK flip-flop.

3) Dynamic Analysis Versus a Frequency Step: A dynamic analysis of the synthesizer versus step variations of the division order N has been carried out. From this analysis, it is possible to obtain the pull-out margin [1]–[7] in terms of the division-order step $\Delta\mathrm{N}$. This margin provides the maximum applicable step $\Delta\mathrm{N_{max}}$ for reaching phase locking without cycle skipping. The maximum value $\Delta\mathrm{N_{max}}$ depends on the location of the synthesizer operating point in the bifurcation diagram. An example is shown in Fig. 6. The phase-locked synthesizer initially operates at the 2.5-GHz output frequency. In Fig. 6(a), a step $\Delta\mathrm{N}=13$ is applied to the frequency divider, making the system evolve to a new phase-locked solution at the output frequency 2.513 GHz, without cycle skipping. In Fig. 6(b), a bigger division-order step

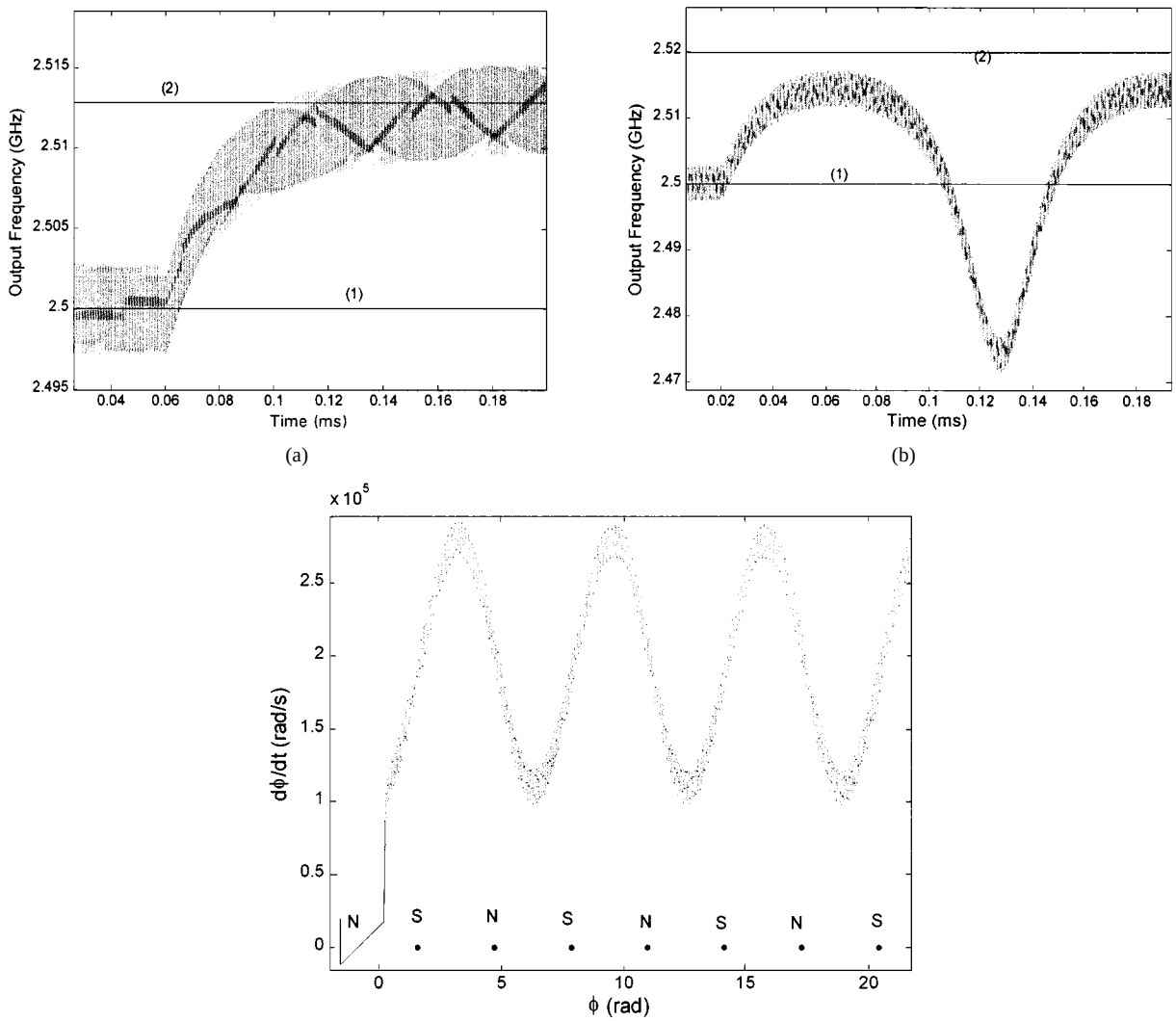

Fig. 6. Dynamic analysis versus a division-order step $\Delta \mathrm{N}$ for parameter values $\mathrm{k_d} = 100\ \mu\mathrm{A}$ and $\mathrm{N} = 2500$. (a) Time evolution for $\Delta \mathrm{N} = 13$. (b) Time evolution for $\Delta \mathrm{N} = 20$. Cycle skipping. (c) Orbit in the phase space $(\phi,\ \dot{\phi})$ for $\Delta \mathrm{N} = 20$.

$\Delta \mathrm{N} = 20$ is applied. Cycle skipping is observed. In this case, phase locking is obtained after a very long transient.

The solution in Fig. 6(b) has also been represented on the plane $(\phi,\ \dot{\phi})$, in Fig. 6(c). Remember that there are two phase-locked solutions lying on the horizontal axis of this plane: i.e., the stable node-type limit cycle $\phi_{\mathrm{n}}(\mathrm{t})$ and the saddle-type limit cycle $\phi_{\mathrm{s}}(\mathrm{t})$. Due to the applied division-order step $\Delta \mathrm{N}$, the orbit suffers a displacement $(\Delta\phi,\ \Delta\dot{\phi})$ from the limit cycle. If the initial displacement $\Delta\dot{\phi}$ is big enough, the unstable manifold of the saddle solution will initially repel the orbit as the phase value increases (due to its time dependence). This is observed in Fig. 6(c). As time evolves, the orbit is then attracted by the node-type limit cycle (thus, it approaches the horizontal axis) and is repelled again by the saddle-type limit cycle. Note the phase difference 2π (horizontal axis) between two consecutive minima or two consecutive maxima of the oscillation. This is also the distance between two consecutive node-type solutions or two consecutive saddle-type solutions.

Fig. 7 shows the variation of the maximum division-order step $\Delta \mathrm{N}_{\max}$ that can be applied to the synthesizer versus the loop gain $\mathrm{k_d}$. Since this step depends on the operating-point position in the bifurcation diagram, the analysis has been particularized to two initial values of the division order: i.e., $\mathrm{N} = 2100$ and $\mathrm{N} = 2500$. As can be seen, the maximum allowed step increases with the output current $\mathrm{k_d}$.

B. Synthesizer With a Digital PD (JK)

When the output current of the PD is modeled by (13), the synthesizer equations become

$$\begin{aligned} \ddot{v} + B\dot{v} + Cv &= \frac{\tau_1}{\tau_2\tau_3}\frac{di}{dt} + \frac{1}{\tau_2\tau_3}\, i \\ &= \pm\frac{kd}{\tau_2\tau_3} \\ \dot{\phi}(t) &= \frac{\Delta\omega}{N} - \frac{k_1}{N}\mathrm{tgh}[k_v v(t)]. \end{aligned} \tag{20}$$

The sign of the right-hand side of the first equation depends on both $\phi(\mathrm{t})$ and $\omega_{\mathrm{i}}\mathrm{t}$ and this dependence is given by (13). The system (20) can be seen as a time-varying system with a memory

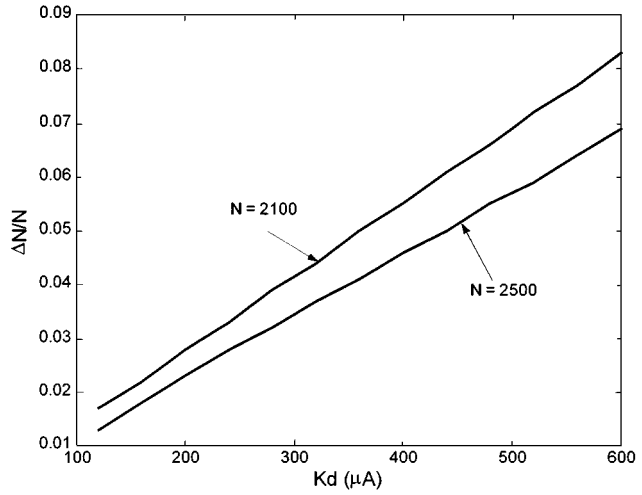

Fig. 7. Pull-out diagram, in terms of division order step ΔN_{max}, for two different initial values of N.

introduced by the sequential flip-flop and with an external input of frequency ω_i.

It must be taken into account that, due to the time discontinuity of the PD, its characteristic is highly nonlinear and will give rise to an infinite number of intermodulation products of the two input frequencies.

1) Nonlinear Dynamics: In locked conditions, the solutions of (20) are given by a couple of time-varying solutions with very small amplitude $\phi_n(t)$, $\phi_s(t)$. Due to the time varying character of (20), in steady state, the fundamental frequency of these solutions is given by the external frequency ω_i. However, for some parameter values, a low-frequency oscillation is also observed [1]. This oscillation plays a determinant role in the system dynamics. In [1, Bibliography], its experimental observation has been related to the phase-margin of the synthesizer-linearized equations. This oscillation cannot generally be predicted through a linear analysis. In Fig. 8(a), a linear simulation of the synthesizer has been carried out for parameter values $N = 2500$ and $k_d = 70\ \mu$A. No low-frequency oscillation is observed. For the same parameter conditions, the nonlinear analysis provides the solution of Fig. 8(b). Two frequencies are involved in this solution: the external frequency ω_i and the low frequency ω_a, which is not observed in Fig. 6(a). The oscillation at ω_a in Fig. 8(b) is, in fact, attenuated after an extremely long transient, whose duration depends on the loop parameters and may be of the order of seconds. As the filter pole approaches the origin, the transient duration tends to infinitum, the oscillation at ω_a becoming a steady state when the pole is located exactly at the origin $\varepsilon = 0$. The value of the frequency ω_a is also dependent on ε, decreasing as the pole approaches the origin.

In practice, for very long transients to the limit cycle at ω_i, the low-frequency oscillation ω_a will be experimentally observable, due to the noise influence. In fact, any arbitrarily small noise perturbation continuously interrupts the evolution to the weakly attracting limit cycle at ω_i, preventing the system from reaching this cycle and maintaining it in the long transient state. This will give rise to FM sidebands at ω_a (very close to the carrier) and at ω_i. This will be shown in more detail in Section V. Note that it

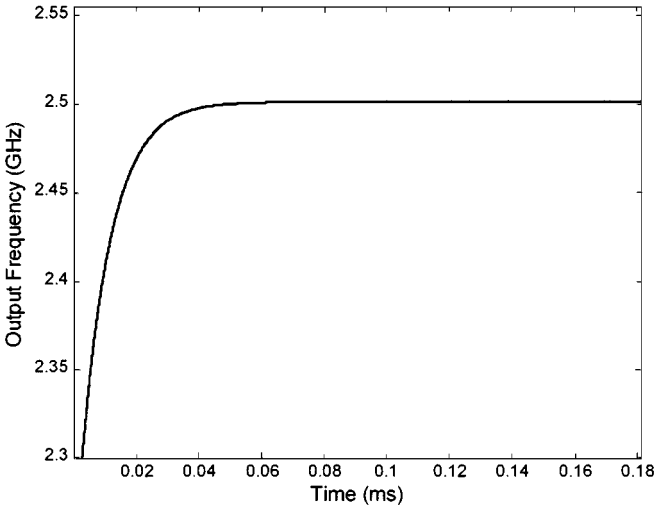

(a)

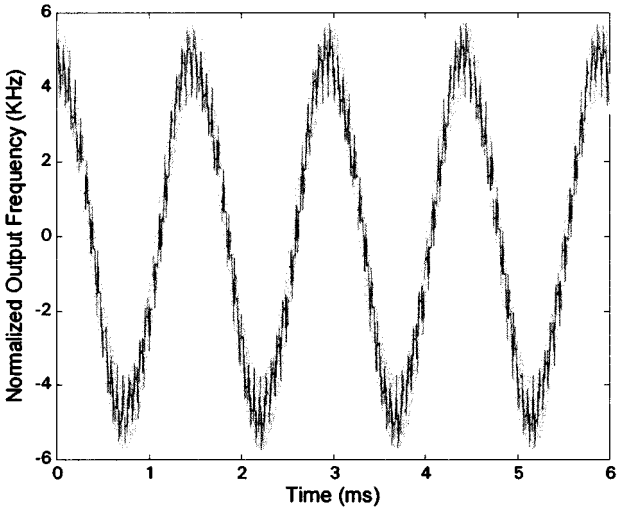

(b)

Fig. 8. Synthesizer output frequency when using a JK PD. Parameter values $k_d = 70\ \mu$A, $N = 2500$. (a) Linearized system. Asymptotic evolution to phase locking. (b) Nonlinear system. Low —frequency modulation of the phase-locked state.

would not have been possible to obtain this spurious frequency if the phase-detector characteristic (12) had been considered, instead of (13). This is an equivalent situation to the one obtained in the case of a frequency mixer when only the phase difference term is taken into account. Under this assumption, the synthesizer phase-locked solutions are given by constant phase values.

The parameter region for which the phase-locked solution $\phi_n(t)$ exists is bounded by the curve at which a collision between the two solutions $\phi_n(t)$ and $\phi_s(t)$ takes place, in an equivalent phenomenon to the one given by (16). This collision provides the synthesizer *hold-in* range (Fig. 9). Thus, phase-locked solutions $\phi_n(t)$ exist on the left-hand side of this border (regions I–III). The border between regions III and IV (*lock-in* border) is given by the *saddle-connection* curve. Rotation solutions are observed in regions III and IV, in the former region coexisting with the phase-locked solutions. As will be shown in the following section, not all the phase-locked solutions in Fig. 9 will be stable.

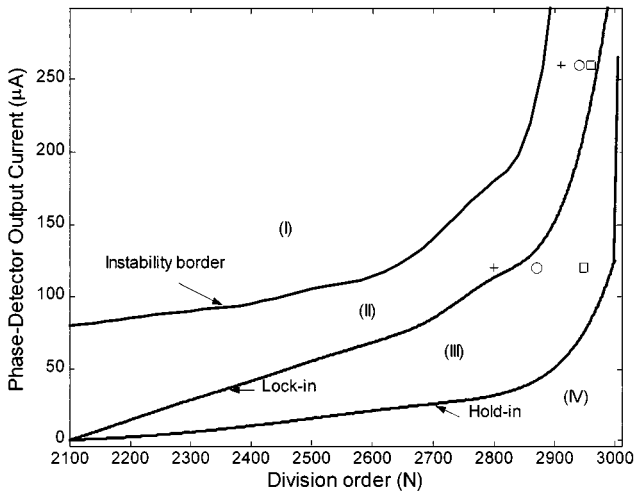

Fig. 9. Bifurcation diagram of the synthesizer when the JK phase detector is used. Region I, unstable phase-locked solutions. Chaos is observed. Region II, stable phase-locked solutions. Region III, coexistence of stable phase-locked solutions and rotations. Region IV, rotations. Measurements have been superimposed for the available current values of the phase-detector.

2) Stability Analysis—Chaotic Responses:

a) Equilibrium-point stability analysis—Root locus: As has been shown, when the phase-detector model (12) is used, the phase-locked solutions are given by constant values of the phase error $\phi = \phi_{\rm on}$. The stability analysis of these solutions is carried out through linearization about $\phi = \phi_{\rm on}$. In order to determine the stability evolution versus variations in a parameter, such as the phase-detector output current $\rm k_d$, the synthesizer root locus can be traced. This has been done in Fig. 10(a) for the synthesizer analyzed here. The division order has been fixed to $\rm N = 2100$. When increasing the output current from $\rm k_d = 0\ \mu A$ to $\rm k_d = 800\ \mu A$, the system poles evolve in the sense indicated by the arrows. From $\rm k_d = 262\ \mu A$, the two poles are complex conjugate. Since the poles are always located on the left-hand side of the complex plane, the system is stable for any $\rm k_d$ value. However, in this analysis, it has not been taken into account that the phase-locked solutions are, in fact, time-varying solutions.

b) Limit-cycle stability analysis—Floquet multipliers: Since the steady state to which the slow transient evolves is a limit cycle at the frequency $\omega_{\rm i}$, the system, under small perturbations, can be linearized about this cycle. The cycle stability can then be determined from Floquet's theory [11].

In (19), the nonlinear system of differential equations of the general synthesizer was written as

$$\dot{\overline{\rm x}} = {\rm F}(\overline{\rm x},\ {\rm t}) \tag{21}$$

where $\overline{\rm x}$ is the state-variable vector containing the phase error and its time derivatives. For the third-order synthesizers that are analyzed here, the dimension of system (21) is $n = 3$. Note that, as observed in (18) and (20), F is periodic in t, with period T. The periodic solution at $\omega_{\rm i}$ is denoted $\overline{\rm x}({\rm t}) = \overline{\rm x}_0({\rm t})$. For its stability analysis, a small perturbation $\overline{\rm u}({\rm t})$ is considered, the corresponding perturbed solution being $\overline{\rm v}({\rm t}) = \overline{\rm x}_0({\rm t}) + \overline{\rm u}({\rm t})$.

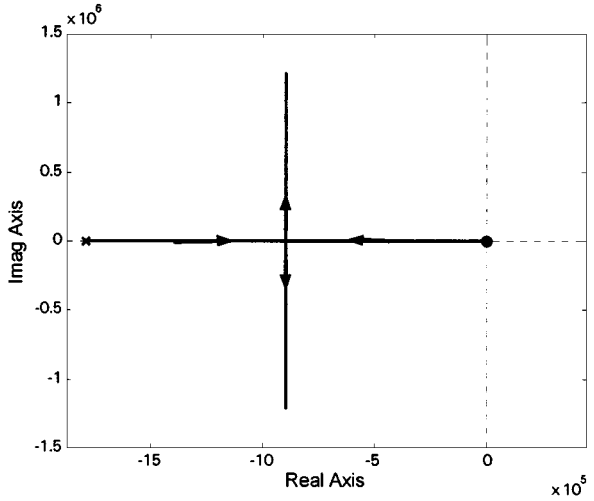

(a)

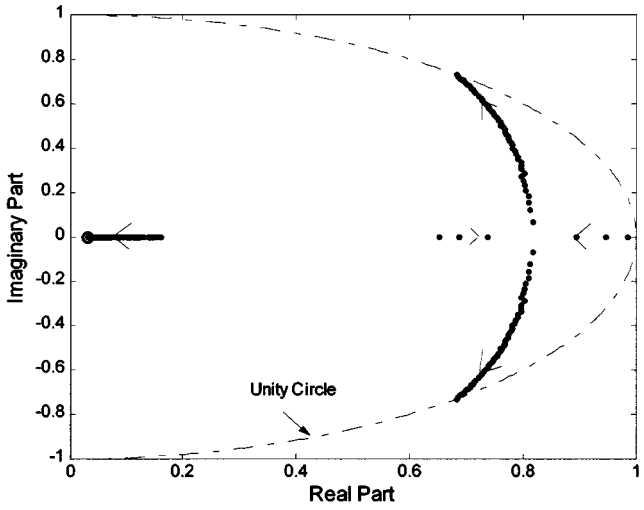

(b)

Fig. 10. Stability analysis of the phase-locked solution versus the phase-detector gain $\rm k_d$ (increasing in the arrow sense). (a) Root locus of the linearized system around the EP. (b) Evolution of the Floquet multipliers. Filter parameters: $\tau_1 = 18\ 10^{-4}\ {\rm s}^{-1}$, $\tau_2 = 2.2\ 10^{-7}\ {\rm s}^{-1}$, $\tau_3 = 5.6\ 10^{-7}\ {\rm s}^{-1}$, $\rm B = 1.8\ 10^6\ s$, $\rm C = 2.7\ 10^7\ s^2$.

The vector $\overline{\rm v}({\rm t})$ is now introduced in the synthesizer equation (21) as follows:

$$\dot{\overline{\rm x}}_0({\rm t}) + \dot{\overline{\rm u}}({\rm t}) = {\rm F}\big(\overline{\rm x}_0({\rm t}) + \overline{\rm u}({\rm t}),\ {\rm t}\big). \tag{22}$$

For a small perturbation $\overline{\rm u}({\rm t})$, the following linearization holds during at least one period T:

$$\dot{\overline{\rm x}}_0({\rm t}) + \dot{\overline{\rm u}}({\rm t}) \approx {\rm F}\big(\overline{\rm x}_0({\rm t}),\ {\rm t}\big) + {\rm D_X F}\big(\overline{\rm x}_0({\rm t}),\ {\rm t}\big)\overline{\rm u}({\rm t}). \tag{23}$$

Thus, the evolution of the perturbation is governed by the linear equation

$$\dot{\overline{\rm u}}({\rm t}) = {\rm A}({\rm t})\overline{\rm u}({\rm t}) \tag{24}$$

with ${\rm A}({\rm t}) = {\rm D_X F}(\overline{\rm x}_0({\rm t}),\ {\rm t})$. Equation (24) represents a linear system of dimension n with time-dependent periodic coefficients. A matrix $\Psi({\rm t})$ composed of n linearly independent solutions of (24) can be obtained, such that any solution of (24) can be expressed as $\overline{\rm u}({\rm t}) = \Psi({\rm t}){\rm C}$, with C an n-dimension vector

of constants. Note that the solution of (24) does not have to be periodic. The matrix $\Psi(t)$ is not unique. For a particular choice $\Psi(t) = \Phi(t)$, fulfilling $\Psi(0) = I$, with I the identity matrix, it can be demonstrated [11] that every solution of (24) can be expressed as

$$\overline{u}(t) = \Phi(t)\overline{u}(0) \tag{25}$$

and for $t = T$

$$\overline{u}(T) = \Phi(T)\overline{u}(0). \tag{26}$$

The matrix $\Phi(t)$ is called the *monodromy* matrix of the system (24). Equation (26) shows that the perturbation value after one period $\overline{u}(T)$ is a linear application of its initial value $\overline{u}(0)$. Being $\{m_i\}_{i=1}^{n}$ the eigenvalues of $\Phi(T)$, if

$$|m_i| \leq 1, \qquad \text{for } i = 1, \ldots, n \tag{27}$$

then, for any initial value $\overline{u}(0)$ of the perturbation, it can be shown that

$$\|\overline{u}(T)\| \leq \|\overline{u}(0)\|. \tag{28}$$

After an infinite number of periods (time tending to infinite), the perturbation value is given by $\overline{u}(nT) = \Phi(T)^n\overline{u}(0)$, $n \to \infty$. Thus, (27) implies that the perturbation $\overline{u}(t)$ vanishes and the synthesizer steady-state solution $\overline{x}_0(t)$ is stable. The values $\{m_i\}_{i=1}^{n}$ are the so-called *Floquet multipliers* [11] associated to $\overline{x}_0(t)$. In general, they are complex values. If any of the multipliers has a module greater that unity, then $\overline{x}_0(t)$ is unstable.

The former analysis has been applied here to the JK-based synthesizer, fixing the division order to $N = 2100$ and increasing k_d, which constitutes the analysis parameter. The resulting evolution of the Floquet multipliers is shown in Fig. 10(b). Initially, the three multipliers are inside the unit circle, which means stable behavior. For low k_d values, the three multipliers are real, lying on the real axis. In similar way to what has already been observed in the root locus, two of the three multipliers become complex conjugate as k_d is increased. Note that when the complex-conjugate multipliers are inside the circle, the low-frequency oscillation vanishes after a long transient, as indicated in the previous paragraph. For $k_d = 80$ μA, the pair of complex-conjugate multipliers leave the unity circle, which implies a bifurcation of Hopf type. When this happens, the phase-locked solution $\phi_n(t)$ is no longer stable.

From the Floquet stability analysis, the diagram showing the global dynamics of the synthesizer on the two-parameter plane can now be completed with a bifurcation locus providing the instability border of the phase-locked solutions (Fig. 9).

Fig. 11 shows the time evolution of the synthesizer solution for parameter values $N = 2100$ and $k_d = 100$ μA. For these values, the standard stability analysis of Fig. 10(a) had predicted stable behavior. The Floquet-multiplier analysis has predicted instability. As can be seen, the amplitude of the low-frequency oscillation increases in time, until the solution collides with the attracting manifold of a chaotic solution. The existence of this chaotic solution is probably due to the fact that three different

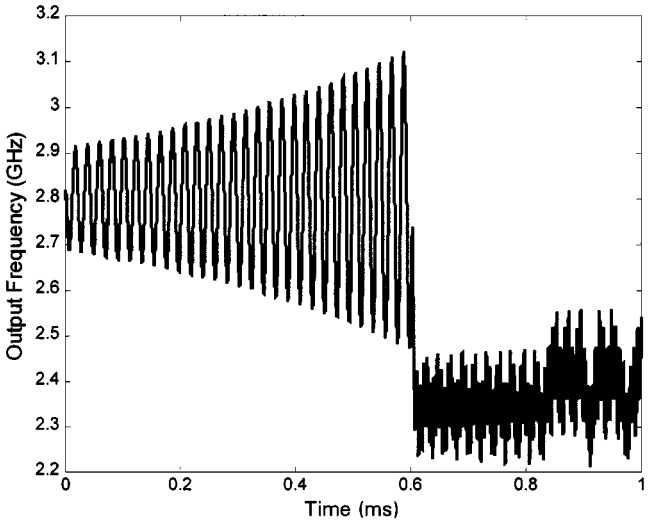

Fig. 11. Parameter values $k_d = 200$ μA and $N = 2800$. Unstable solution. Collision with the stable manifold of a chaotic attractor.

fundamentals are involved in the system [12]: i.e., the reference frequency, the VCO output frequency, and the low oscillation frequency $\omega_a$mentioned above.

When analyzing a type-I PLL with a frequency modulated input, other authors [2], [3] have encountered chaotic solutions due to the formation of transversal homoclinic orbits. This does not seem to be the case here. Actually, the chaotic solutions in region I (Fig. 9) are observed after the occurrence of a nontransversal *saddle connection*. In this study, two different chaotic attractors have been obtained: i.e., one located below the straight line $\dot{\theta}_o = N\omega_i$ and the other above this frequency value. As k_d is increased, both attractors increase in size. They approach and intermittent transitions are observed between them. As the gain continues to increase, they become a single chaotic attractor.

The chaotic solution to which the system evolves in Fig. 11 is responsible for the observation of unlocked states within the synthesizer *hold-in* ranges. Fig. 12 shows the simulated and measured spectrum for the same parameter conditions $N = 2100$ and $k_d = 150$ μA. Note that, for calculation simplicity, the simulated spectrum is obtained at the frequency-divider output instead of the VCO output.

The frequency peak deviation, due to the chaotic operation, and pull-in time (calculated as the rise time to a first zero value of the frequency error) are plotted in Fig. 13 versus the phase-detector output current.

IV. Phase-Noise Analysis

A. Output Spectrum in Phase-Locked Conditions

In order to analyze the influence of noise perturbations on the synthesizer behavior, the loop-element noise contributions have been included in the analysis. Note that, if the sidebands inherent to the synthesizer solution are to be taken into account for this analysis, the standard linearization around the EP $\phi = \phi_{on}$ is not applicable. In phase-locked conditions, use can be made of the complex-envelope representation of the VCO output signal, which is outlined in the following. This representation is used

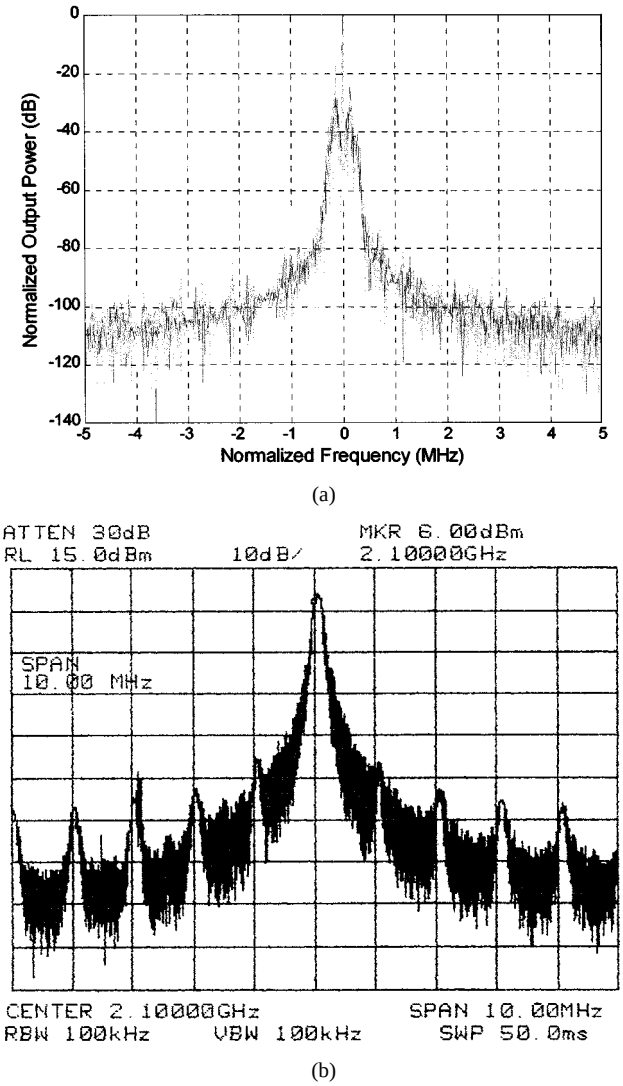

Fig. 12. Chaotic spectrum for $N = 2100$. (a) Simulated at the frequency-divider output. (b) Measured at the VCO output.

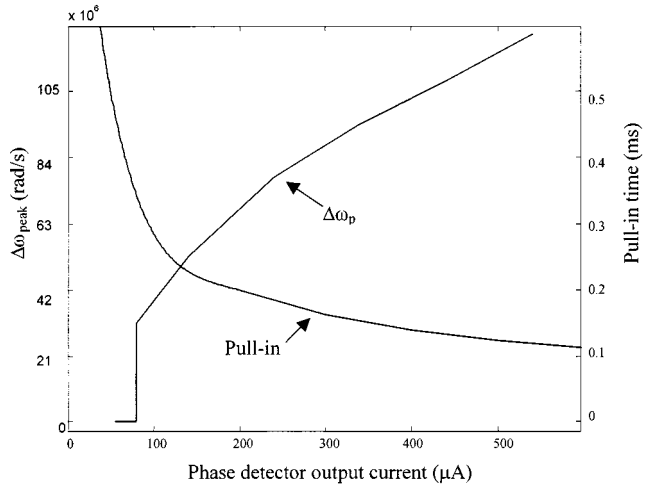

Fig. 13. Peak frequency deviation and pull-in time versus phase-detector output current. Discontinuity is due to the chaos onset. $N = 2100$.

for the determination of the synthesizer phase noise at the VCO output.

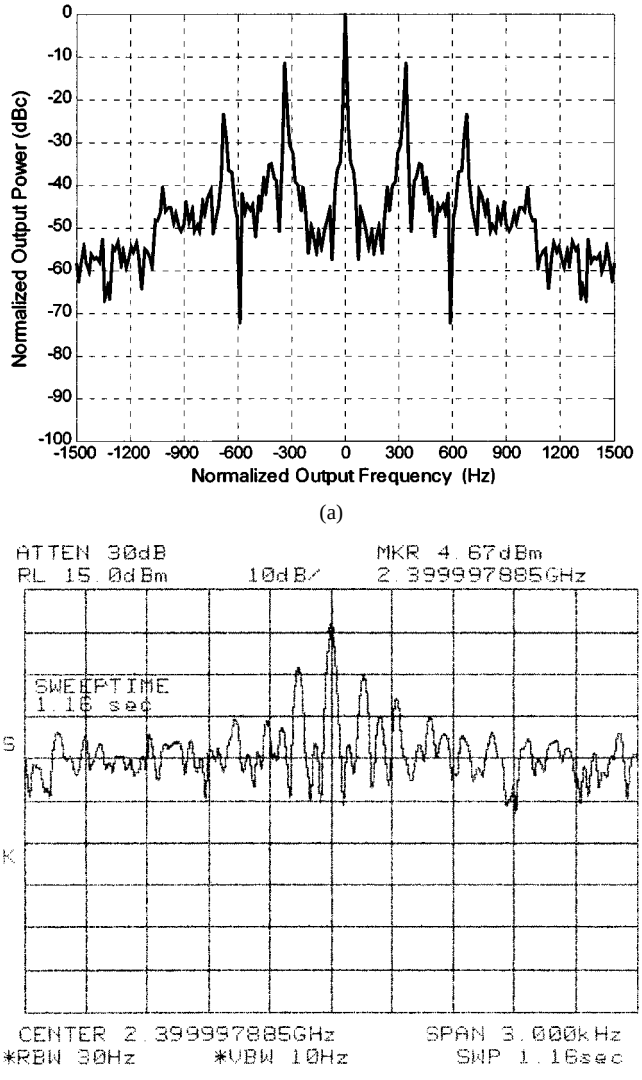

Fig. 14. Synthesizer output spectrum when noise perturbations are considered. Parameter values $k_d = 70\ \mu A$ and $N = 2400$. (a) Simulated. (b) Experimental.

1) Complex-Envelope Representation of the VCO Output: In phase-locked conditions, the spectrum at the VCO output can be calculated using a complex-envelope representation of the VCO output signal [13]. Note that when the system is in the locked state, the frequency modulation gives rise to a narrow spectrum centered around the carrier at $N\omega_i$. In this case, the VCO output signal can be expressed as follows:

$$\begin{aligned} v_o(t) &= \cos[\theta_o(t)] \\ &= \cos\left[N\omega_i t - N\phi(t)\right] \\ &= x(t)\cos(N\omega_i t) + y(t)\sin(N\omega_i t) \end{aligned} \tag{29}$$

with $\phi(t)$ being the phase error and $x(t) = \cos[N\phi(t)]$ and $y(t) = \sin[N\phi(t)]$.

If the modulation peak is not too big, the signals $x(t)$ and $y(t)$ will vary slowly with time. The spectral components of $v_o(t)$ (denoted here as Fv_o) can then be obtained using the expression [14]

$$Fv_o(N\omega_i + \omega) = \frac{Fx(\omega) - iFy(\omega)}{2} \tag{30}$$

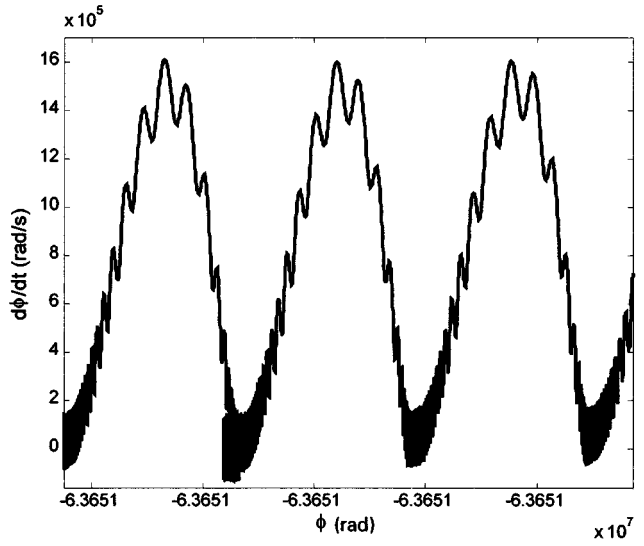

Fig. 15. Stochastic resonance. Parameter values $N = 2900, k_d = 120\ \mu A$. Solution trajectory in the phase space.

where ω is the small frequency offset from the carrier (*normalized frequency*) and $F_x(\omega)$, $F_y(\omega)$ are, respectively, the spectral components of $x(t)$ and $y(t)$. Note that as the modulation peak increases, the spectra of $x(t)$ and $y(t)$ broaden and the sampling interval has to be reduced. When the band is too broad, this method is not applicable. Thus, it cannot be applied to chaotic solutions.

2) Phase-Noise Calculation: Here, a nonlinear analysis in the presence of phase-noise fluctuations in the reference oscillator and the VCO has been carried out. The phase-noise contribution from these two elements has been experimentally characterized. From the measured phase-noise spectral density, a time-domain noise model has been obtained. This is composed of a white-noise source, plus a filter, with a frequency response that fits the experimental results [15]. The spectrum has been calculated by making use of the periodogram technique [16].

When a JK-based PD is used, the locked solution is a stable limit cycle at frequency ω_i. According to the loop parameters, the transient state may also exhibit a small frequency damped oscillation at ω_a. However, due to the proximity to the critical value $\varepsilon = 0$, the damping ratio is very low and the continuous perturbation by noise makes observable the characteristics of the transient. Thus, the spectrum of the phase-locked state will have noise sidebands at ω_i and ω_a. It is an example of a noisy precursor [17].

Since ω_a is very small, the sidebands due to this frequency are very close to the carrier. They are the so-called "noise ears" [1]. The simulated output spectrum is given in Fig. 14(a). The corresponding measured spectrum is shown in Fig. 14(b). Note that, in the simulation case, the output power has been normalized. Both in simulation and experiment, the sideband power is 10 dB below the carrier power. In both cases, the sideband frequency offset is in the order of 100 Hz. The slight discrepancy is due to errors in the filter modeling since the value of the frequency ω_a is strongly dependent on the filter pole distance to the origin ε. When the filter pole approximates the origin, the amplitude

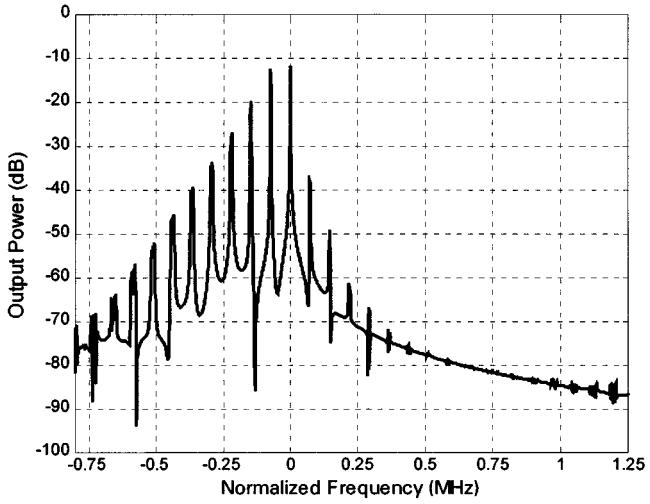

(a)

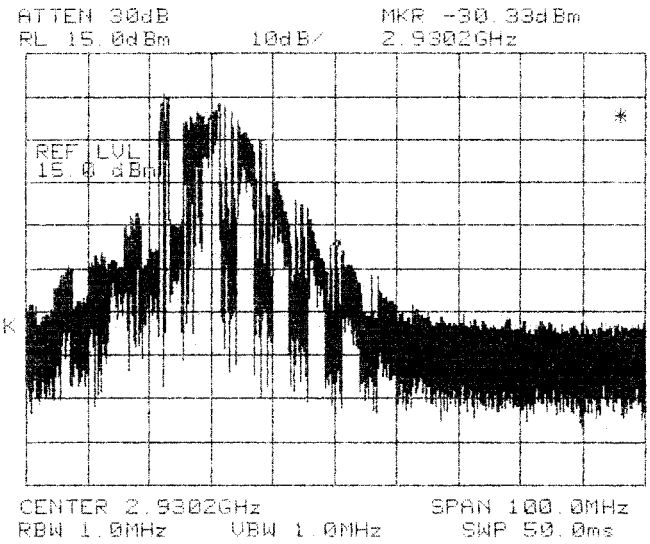

(b)

Fig. 16. Stochastic resonance. Parameter values $N = 2900, k_d = 120\ \mu A$. (a) Simulated spectrum at the frequency-divider output. (b) Measured spectrum at the VCO output.

of noise bands near to the carrier grows and they approach the carrier.

B. Stochastic Resonance

As has been shown, stable rotation solutions and phase-locked states coexist for some parameter ranges of the synthesizer. This region is limited by two bifurcation loci: i.e., the *saddle-node* curve and the *saddle-connection* curve. In the neighborhood of the *saddle-connection* curve (*lock-in* border), the phase-locked states and rotation-type solutions are very close. Thus, under the influence of noise perturbations, intermittent transitions between locked and unlocked states can be observed. This phenomenon, known as *stochastic resonance* [18], [19], has been experimentally observed in the synthesizer analyzed here. The digital circuitry informing about the synthesizer state intermittently signaled *locked* and *unlocked* behavior. This corresponds to transitions between a rotation and a phase-locked limit cycle. The time-domain trajectory

under noise perturbations for parameter values $N = 2900$ and $k_d = 150\ \mu$A (very close to a saddle connection) is shown in Fig. 15. The short-duration phase locking takes place in the dense intervals located about $\dot{\phi} = 0$. The system then moves to the rotation solution, returning after a short time interval to the phase-locked state. This gives rise to a great increase in the noise-power spectral density, as shown in the simulated spectrum of Fig. 16(a), obtained at the frequency divider output. Fig. 16(b) shows the measured spectrum at the VCO output for the same operation conditions.

Note that the analysis of the stochastic resonance is impossible under system-linearization conditions. The linearization assumes a small variation of the system state variables under the noise perturbation. Close to a bifurcation point, this is no longer true, as in the example of Fig. 15.

V. Conclusions

A global analysis of the nonlinear dynamics of microwave frequency synthesizers based on type-II PLLs has been presented. The analysis is based on a realistic description of the synthesizer elements, which has enabled the accurate determination of its operating borders and, thus, the prediction of hysteresis phenomena. Two different kinds of PD have been considered: i.e., a digital PD, based on a JK flip-flop, and a typical analog mixer. The performances of both are compared in terms of stability and spurious components in the output spectrum. Prediction of incidental FM noise is also carried out. Its influence on the VCO output spectrum is quantified by means of a nonlinear analysis of the synthesizer, in the presence of noise perturbations. This nonlinear analysis has enabled the detection of stochastic resonance in type-II loop synthesizers, commonly observed in practice. The analysis results have been compared with the experimental ones in a synthesizer based on a 2–3-GHz VCO.

References

[1] U. L. Rohde, *Microwave and Wireless Synthesizers*. New York: Wiley, 1997.

[2] F. M. A. Salam and S. Shankar Sastry, "Dynamics of the forced Josephson-junction circuit: The regions of chaos," *IEEE Trans. Circuits Syst.*, vol. CT-32, pp. 784–796, Aug. 1985.

[3] T. Endo and L. O. Chua, "Chaos from phase-locked loops," *IEEE Trans. Circuits Syst.*, vol. 35, pp. 987–1003, Aug. 1988.

[4] M. Odyniec and L. O. Chua, "Josephson-junction circuit analysis via integral manifolds," *IEEE Trans. Circuits Syst.*, vol. CT-30, pp. 308–320, May 1983.

[5] F. M. Gardner, *Phaselock Techniques*. New York: Wiley, 1966.

[6] V. Manassewitsch, *Frequency Synthesizers: Theory and Design*. New York: Wiley, 1987.

[7] A. Viterbi, "Acquisition and tracking behavior of phase-locked loops," JPL, Pasadena, CA, Ext. Pub. 673, July 1959.

[8] R. Sanneman *et al.*, "Unlock characteristics of the optimum type II phase-locked loop," *IEEE Trans. Aerosp. Navig. Electron.*, vol. ANE-11, pp. 15–24, Mar. 1964.

[9] S. Sancho, A. Suárez, and T. Fernández, "Nonlinear analysis of microwave frequency synthesizers: Stability and incidental FM," in *Proc. IEEE MTT-S Int. Microwave Symp. Dig.*, 2000, pp. 497–500.

[10] S. Wiggins, *Introduction to Applied Nonlinear Dynamical Systems and Chaos*. Berlin, Germany: Springer-Verlag, 1990.

[11] G. Ioos and D. D. Joseph, *Elementary Stability and Bifurcation Theory*, 2nd ed. Berlin, Germany: Springer-Verlag, 1990.

[12] J. M. T. Thompson and H. B. Stewart, *Nonlinear Dynamics and Chaos*. New York: Wiley, 1986.

[13] L. R. Rabiner and B. Gold, *Theory and Application of Digital Signal Processing*. Englewood Cliffs, NJ: Prentice-Hall, 1975.

[14] W. R. Bennet, "Methods of solving noise problems," *Proc. IRE*, vol. 44, pp. 609–638, May 1956.

[15] A. B. Carlson, *Communication Systems*. New York: McGraw-Hill, 1986.

[16] E. O. Brigham, *The Fast Fourier Transform and Its Applications*. Englewood Cliffs, NJ: Prentice-Hall, 1988.

[17] C. Jeffries and K. Wiesenfeld, "Observation of noisy precursors of dynamical instabilities," *Phys. Rev. A, Gen. Phys.*, vol. 31, pp. 1077–1084, 1982.

[18] F. Moss, D. Pierson, and D. O'Gorman, "Stochastic resonance: Tutorial and update," *Int. J. Bifurcations Chaos*, vol. 4, no. 6, pp. 1383–1397, June 1994.

[19] V. S. Anishchenko, M. A. Safonova, and L. O. Chua, "Stochastic resonance in the non autonomous Chua's circuit," *J. Circuits, Syst., Comput.*, vol. 3, no. 2, pp. 553–578, Feb. 1993.

Sergio Sancho was born in Santurce, Spain, in 1973. He received the Physics degree from the Basque Country University, Vizcaya, Spain, in 1997, and is currently working toward the Ph.D. degree in electronic engineering at the University of Santander, Santander, Spain.

His research interests are nonlinear systems, chaos, and the study of the influence of noise in such systems.

Almudena Suárez (M'96) received the Electronic Physics degree and the Ph.D. degree from the University of Cantabria, Cantabria, Spain, in 1987 and 1992, respectively, and the Ph.D. degree in electronics from the University of Limoges, Limoges, France, in 1993.

Since 1995, she has been an Associate Professor at the University of Cantabria, Santander, Spain, where she is a member of the Communications Engineering Department. Her areas of interest include the nonlinear design of microwave circuits, especially the nonlinear stability analysis and investigation of chaotic regimes. She is currently the project manager of a Spanish national research and development project and has taken part in a number of Spanish and European projects in collaboration with industries.

Tomás Fernández was born in Torrelavega, Spain, in 1966. He received the Physics degree and the Doctor of physics degree from the University of Cantabria, Santander, Spain, in 1991 and 1996, respectively.

Since 1998, he has been a Lecturer in the Communications Engineering Department, University of Cantabria. His past and current research interests include large-signal nonlinear modeling of III–V compounds transistors and Si–Ge heterojunction bipolar transistors (HBTs). His research is currently focused on the problem of behavior dependence of such devices on thermal and frequency effects. He has participated in several researching projects (i.e., ESPRIT, TMR, etc.), as well as industrial RF and microwave projects with Spanish and European Companies.